arXiv:1511.01403v1 [cond-mat.quant-gas] 4 Nov 2015

Two-field optical methods to control magnetic Feshbach resonances

A. Jagannathan[1,2], N. Arunkumar[1], J. A. Joseph[1], and J. E. Thomas[1]
[1] *Department of Physics, North Carolina State University, Raleigh, NC 27695 and*
[2] *Department of Physics, Duke University, Durham, NC 27708*
(Dated: November 5, 2015)

Using an optically-trapped mixture of the two lowest hyperfine states of a ^{6}Li Fermi gas, we observe two-field optical tuning of the narrow Feshbach resonance by up to 3 G and an increase in spontaneous lifetime near the broad resonance from 0.5 ms to 0.4 s. We present a new model of light-induced loss spectra, employing continuum-dressed basis states, that agrees in shape and magnitude with measurements for both broad and narrow resonances.

PACS numbers: 03.75.Ss

Optical control methods offer tantalizing possibilities for creating "designer" two-body interactions in ultracold atomic gases, with both high spatial resolution and high temporal resolution. By controlling the elastic scattering length, the inelastic scattering length, and the effective range, optical methods enable control of few-body and many-body systems, opening new fields of research.

Single optical field methods have been used to control Feshbach resonances, with large detunings to suppress spontaneous scattering, leading to limited tunability [1–9]. The first experiments, by Lett and collaborators in a Na Bose gas, demonstrated optically-induced Feshbach resonances, coupling the ground and excited molecular states in the input channel [3]. Recently, Chin and coworkers observed suppression of both spontaneous scattering and the polarizability of Cs atoms, by tuning between the D1 and D2 lines [9]. This method suppresses unwanted optical forces and achieves a lifetime up to 100 ms with rapid but limited tuning, by modulating the intensity of the control beam.

Building on ideas suggested by Bauer et al., [7] and by Thalhammer et al., [10], we are developing two-field optical control methods [11, 12] that create a molecular dark state in the closed channel of a magnetic Feshbach resonance, as studied recently in dark state spectroscopy [13]. This approach is closely related to electromagnetically induced transparency (EIT) [14], where quantum interference suppresses unwanted optical scattering. In contrast to single field methods, our two-field methods are applicable to broad Feshbach resonances, as they produce relatively large tunings for a given loss rate. Further, the two-field methods produce narrow energy-dependent features in the scattering phase shift, enabling control of the effective range [12]. Analogous to the EIT method of enhancing optical dispersion in gases with suppressed absorption [14], the effective range can be modified in regions of highly suppressed optical scattering.

Implementation of optical control methods requires an understanding of the optically-induced level structure and energy shifts, which depend on the relative momentum of a colliding atom pair. Our original theoretical approach [11, 12] and that of other groups [7] employed adiabatic elimination of an excited molecular state amplitude, which fails for very broad resonances where the hyperfine coupling constant is large. This unresolved issue has been noted previously [15].

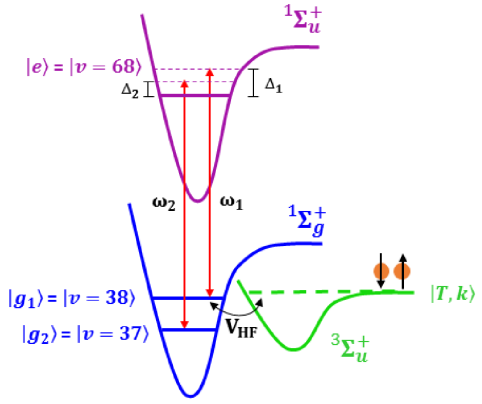

FIG. 1: Basic level scheme for the two-field optical technique. Optical fields of frequencies ω_1 (detuning Δ_1) and ω_2 (detuning Δ_2) , respectively, couple two singlet ground molecular states $|g_1\rangle$ and $|g_2\rangle$ to the singlet excited molecular state $|e\rangle$; V_{HF} is the hyperfine coupling between the incoming atomic pair state in the open triplet channel $|T, k\rangle$ and $|g_1\rangle$, which is responsible for a magnetically controlled Feshbach resonance.

In this Letter, we demonstrate large shifts of magnetic Feshbach resonances and strong suppression of spontaneous scattering in measurements of two-field light-induced loss spectra. Further, we present a new theoretical approach to describe control of broad and narrow Feshbach resonances in a unified manner, replacing a "bare" state description by a more natural description in terms of "continuum-dressed" states that incorporate the hyperfine coupling into the basis states. Using the measured Rabi frequencies, the predicted relative-momentum averaged loss spectra agree in shape and magnitude with data for both broad and narrow resonances.

The basic level scheme for the two-field optical technique is shown in Fig. 1. An optical field with Rabi frequency Ω_1 and frequency ω_1 couples the ground vibrational state $|g_1\rangle$ of the $^1\Sigma_g^+$ potential to the excited

vibrational state $|e\rangle$ of the $^1\Sigma_u^+$ potential. A second optical field with Rabi frequency Ω_2 and frequency ω_2 couples a lower lying ground vibrational state $|g_2\rangle$ to the excited vibrational state $|e\rangle$. The ω_1 beam results in a light shift of state $|g_1\rangle$ as well as atom loss due to photoassociation from the triplet continuum $|T,k\rangle$ to the excited state $|e\rangle$. The ω_2 beam suppresses atom loss through destructive quantum interference. In a magnetic field B, the triplet continuum $|T,k\rangle$ tunes downward $\propto 2\mu_B B$, where μ_B is the Bohr magneton, $\mu_B/h \simeq h \times 1.4$ MHz/G. $|T,k\rangle$ and $|g_1\rangle$ have a hyperfine coupling constant V_{HF}, producing a Feshbach resonance. For our experiments with ^{6}Li, $|g_1\rangle$ and $|g_2\rangle$ are the $v = 38$ and $v = 37$ ground vibrational states and $|e\rangle$ is the $v = 68$ excited vibrational state, which decays at a rate $\gamma_e = 2\pi \times 11.8$ MHz.

The detunings of the optical fields that couple state $|g_1\rangle$ and $|g_2\rangle$ to $|e\rangle$ are Δ_1 and Δ_2, respectively. The single photon detuning of the ω_1 beam for the $|T\rangle \rightarrow |e\rangle$ transition is a function of magnetic field and can be defined at a reference magnetic field B_{ref} as $\Delta_e = \Delta_L - 2\mu_B(B-B_{ref})/\hbar$, where Δ_L is the detuning of the optical field when $B = B_{ref}$. The two-photon detuning for the $|T\rangle - |e\rangle - |g_2\rangle$ system is $\delta = \Delta_e - \Delta_2$.

We prepare a 50:50 mixture of ^{6}Li atoms in the two lowest hyperfine levels, $|1\rangle$ and $|2\rangle$ in a CO_2 laser trap with trap frequencies $(\omega_x, \omega_y, \omega_z) = 2\pi\times(3100, 3350, 120)$ Hz. The $|1\rangle$-$|2\rangle$ mixture of ^{6}Li has a broad Feshbach resonance at $B_\infty = 832.2$ G [17, 18] of width $\Delta B = 300$ G due to strong hyperfine coupling of the triplet continuum to the "broad" singlet state $|g_1\rangle_B$ [12]. In addition, there is a narrow Feshbach resonance at 543.2 G of width ΔB = 0.1 G [19] due to weak second order hyperfine coupling of the triplet continuum $|T\rangle$ to the "narrow" singlet state $|g_1\rangle_N$ [12]. After forced evaporation, and re-raising the trap to full trap depth, we have approximately 10^5 atoms per spin state for our experiments. We generate both the ω_1 and ω_2 beams from diode lasers, locked to a stabilized cavity near 673.2 nm. The relative frequency is $\simeq$ 57 GHz [13] with a jitter $<$ 50 kHz. The absolute frequency stability is $<$100 kHz. Both laser beams are sent through fibers and focused onto the optically-trapped atom cloud with both beams polarized along the bias magnetic field z-axis [16].

Initially, we use a single optical field (ω_1 beam) to observe the shift of the narrow Feshbach resonance in the atom loss spectra. After forced evaporation at 300 G, the magnetic field is swept to the field of interest and allowed to stabilize. Then the ω_1 field is shined on the atoms for 5 ms, with a detuning $\Delta_L = 30.2$ MHz (with $\Delta_L \equiv 0$ for $B = B_{ref} = 543.2$ G), after which the atoms are imaged at the field of interest to determine the density profile and the atom number.

Single field atom loss spectra versus magnetic field, Fig. 2, exhibit two loss peaks: i) A broad peak arises at 554 G, where the ω_1 optical field is resonant ($\Delta_e = 0$) with the $|T\rangle \rightarrow |e\rangle$ transition. Here, the transition arises from the hyperfine coupling of $|T\rangle$ to $|g_1\rangle_B$, far from the resonance at 832.2 G. ii) A narrow peak below 543.2 G occurs as the magnetic field tunes the triplet continuum near $|g_1\rangle_N$, which is light-shifted in energy (to B'_{res}) due to the ω_1 optical field, detuned from the $|g_1\rangle_N \rightarrow |e\rangle$ transition by $\Delta_1 = \Delta_L = 30.2$ MHz (see Fig. 1). In this case, the transition strength is resonant, while the ω_1 optical field is off-resonant with the $|T\rangle \rightarrow |e\rangle$ transition by $\Delta_L = 30.2$ MHz. For a $\Omega_1 = 3.1\gamma_e$, the narrow resonance is shifted downward by 3.0 G, approximately

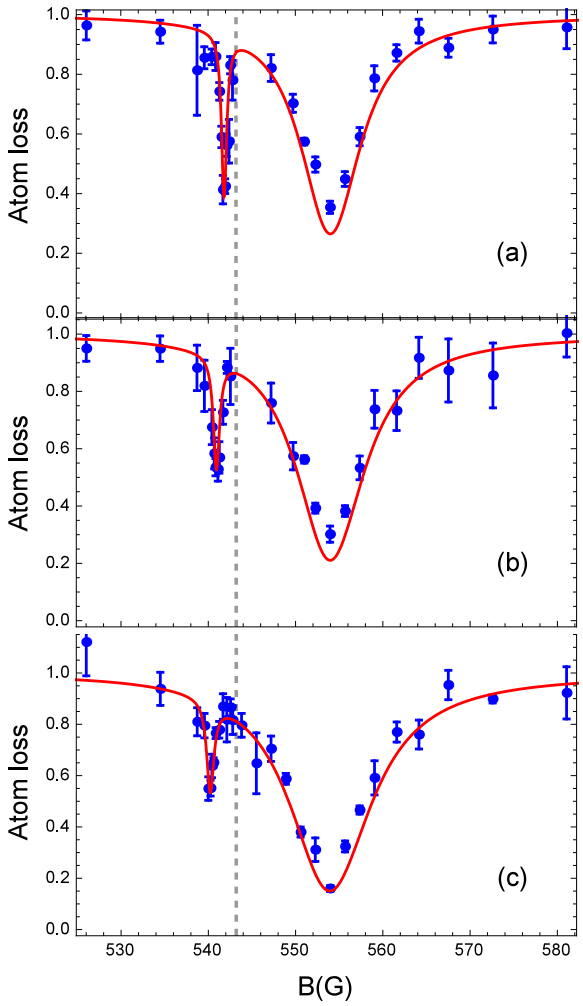

FIG. 2: Shifting the narrow Feshbach resonance at 543.2 G using a single optical field. The large loss peak on the right arises from the broad resonance; The left loss peak arises from the shifted narrow resonance. Vertical dashed line: Position of the unshifted narrow resonance. The background (non-optical) three-body loss near 543.2 G has been suppressed for clarity. Pulse duration $\tau = 5.0$ ms; $T = 5.4\,\mu$K; $\Delta_L = \Delta_1 = 30.2$ MHz; (a) $\Omega_1 = 2.00\,\gamma_e$; $B'_{res} = 541.9$ G (b) $\Omega_1 = 2.65\,\gamma_e$; $B'_{res} = 541.0$ G (c) $\Omega_1 = 3.10\,\gamma_e$; $B'_{res} = 540.2$ G; $\gamma_e = 2\pi \times 11.8$ MHz. Blue dots: Experiment; Solid red curves: Continuum-dressed state model [16].

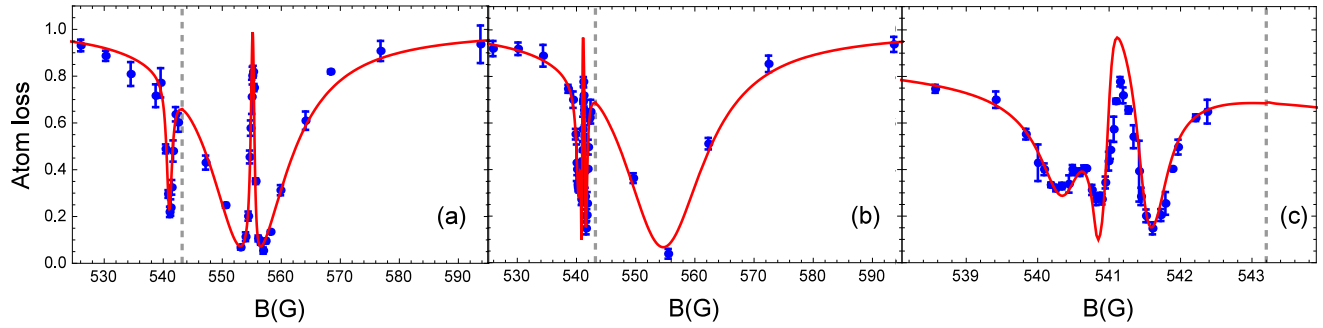

FIG. 3: Loss suppression using the two-field optical technique. The ω_1 beam shifts the narrow Feshbach resonance and the frequency of the ω_2 beam is chosen to suppress loss from (a) the broad resonance (b) the shifted narrow Feshbach resonance; (c) shows an expanded view of (b) near the loss suppression region. Pulse duration $\tau = 5.0$ ms; $T = 4.5\,\mu$K; $\Omega_1 = 2.6\,\gamma_e$; $\Omega_2 = 0.8\,\gamma_e$; $\Delta_L = \Delta_1 = 30.2$ MHz; $B'_{res} = 541.1$ G. Solid red curves: Continuum-dressed state model [16].

30 times the width. The continuum-dressed state model (solid red line), simultaneously reproduces the shift of the narrow resonances and the amplitudes of both the narrow and broad resonances, using the measured Ω_1 [16].

For the two-field loss-induced suppression measurements, Fig. 3, the ω_2 optical field is applied. After sweeping to the magnetic field of interest, the ω_2 beam of intensity of 0.4 kW/cm^2 is adiabatically turned on over 30 ms. The ω_2 beam creates an optical dipole trap and provides additional confinement in the z-direction, due to its high intensity. This changes the axial trap frequency from 120 Hz to 218 Hz, with negligible change in the radial trap frequencies. The ω_1 beam is then turned on for 5 ms, after which both beams are turned off abruptly. The detuning Δ_2 of the ω_2 beam can be chosen to suppress loss either at the broad peak or the narrow peak. For $\Delta_2 = \Delta_e = 0$, the loss is suppressed at the center of the broad peak Fig. 3a. For $\Delta_2 = \Delta_1 + 2\mu_B\,(543.2 - B'_{res})$, the loss is suppressed at the center of the shifted narrow peak, Fig. 3b and 3c. The loss spectra clearly demonstrate the Feshbach resonance can be strongly shifted and that loss can be strongly suppressed using two-field methods. The continuum-dressed state model (red solid curves) predicts the features for all three data sets using the same Rabi frequencies Ω_1 and Ω_2, which are close to the predicted values [16]. We note that the predicted central peaks in Fig. 3c are somewhat larger than the measured values, which may arise from jitter in the two-photon detuning and intensity variation of the Ω_2 beam across the atom cloud.

We have also measured light-induced loss and loss suppression as a function of the ω_1 laser frequency near the broad resonance. Data for $B = 840$ G is shown in Fig. 4. When the ω_1 beam is tuned to achieve two-photon resonance, the loss is highly suppressed. For this experiment, $\Delta_2 = 10$ MHz. Since the maximum suppression occurs for $\Delta_e = \Delta_2$, we observe an asymmetric EIT window. To examine the loss suppression further, we measure the number of atoms as a function of time with the magnetic field tuned to the suppression point. We observe dramatic suppression of loss using the two-field method, achieving an increase of the inelastic lifetime near the broad resonance of ^{6}Li from 0.5 ms with a single laser field to 400 ms with the two-field method, Fig. 5, limited by jitter in the two-photon detuning.

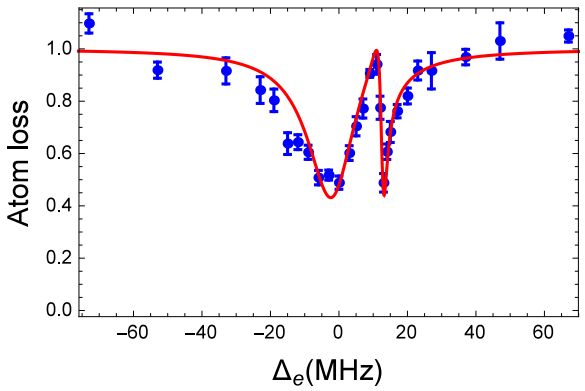

FIG. 4: Loss suppression near the broad resonance at 832.2 G, for $B = 840$ G, as a function of single photon detuning by sweeping the ω_1 laser frequency. Pulse duration $\tau = 5.0$ ms; $T = 14.8\,\mu$K $\Omega_1 = 1.36\,\gamma_e$; $\Omega_2 = 0.9\,\gamma_e$; $\Delta_2 = 10.0$ MHz. Maximum suppression occurs for $\Delta_e = \Delta_2 = 10.0$ MHz, where $\delta_e = 0$. Solid red curve: Continuum-dressed state model [16].

Measured light-induced loss spectra are compared to predictions by calculating the atom loss rate [16]. For a 50-50 mixture of two hyperfine states, the total density decays according to $\dot{n}(\mathbf{r},t) = -\frac{1}{2}\langle K_2(k,\mathbf{r})\rangle\,[n(\mathbf{r},t)]^2$. Here, the angle brackets in $\langle K_2(k,\mathbf{r})\rangle$ denote an average over the relative momentum $\hbar k$ distribution. As the Rabi frequencies that determine K_2 generally vary in space, we

include an additional position dependence in $\langle K_2 \rangle$. For simplicity, we assume in this paper a classical Boltzmann distribution, which is applicable in the high temperature regime employed in the measurements and defer treatment of quantum degeneracy and many-body effects to future work.

The loss rate constant $K_2(k)$ is calculated from the optically-modified scattering state in the continuum-dressed state basis [16]. In previous calculations [7, 11, 12], interaction of the colliding atom pair with the optical fields is described in the "bare" state basis, Fig. 6a, with singlet states, $|g_1\rangle$, $|g_2\rangle$, and $|e\rangle$, and triplet continuum $|T, k\rangle$. Using the continuum-dressed state basis, Fig. 6b, the bare states $|g_1\rangle$ and $|T, k\rangle$, are replaced by the dressed bound state $|E\rangle$ and the Feshbach resonance scattering state $|E_k\rangle$. These dressed states already contain the hyperfine coupling constant V_{HF}, permitting consistent adiabatic elimination of the excited state amplitude $|e\rangle$, even for broad Feshbach resonances where V_{HF} is large. From the scattering state, we determine the corresponding two-body scattering amplitude $f(k)$, which yields $K_2(k)$ from the inelastic cross section. The new model shows that the light-shifts arising from the Ω_1 beam have a different relative momentum (k) dependence for broad resonances than for narrow resonances. Further, it reproduces previous calculations [7, 11, 12] that are valid only for narrow resonances and avoids predictions of a spurious broad resonance at B_∞ that arises when narrow resonance results are incorrectly applied to broad resonances.

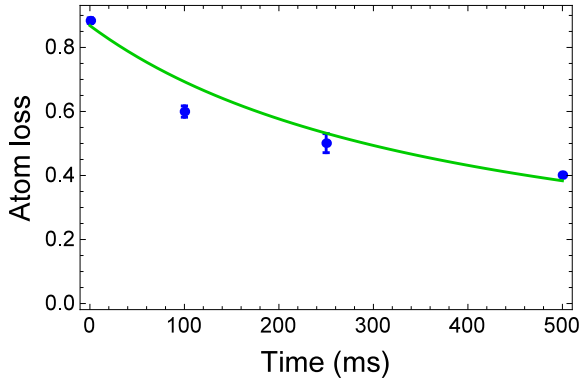

FIG. 5: Number of atoms in state $|1\rangle$ versus time with $\Omega_1 = 0.65\,\gamma_e$ and ω_1 tuned to cause loss at 841 G. $\Omega_2 = 0.9\,\gamma_e$ and ω_2 is tuned to suppress loss near 841 G. With $\Omega_2 = 0$, the corresponding decay time is $\simeq 0.5$ ms. $\gamma_e = 2\pi \times 11.8$ MHz is the radiative decay rate; $T = 4.5\,\mu$K. Solid green curve: $N(t) = N(0)/(1 + \gamma t)$, where $\gamma = 2.5\,s^{-1}$.

In conclusion, we have demonstrated that two-optical field methods can produce large shifts of magnetic Feshbach resonances and strong suppression of spontaneous scattering, enabling flexible control of the trade-off between loss and tunability. We have established a

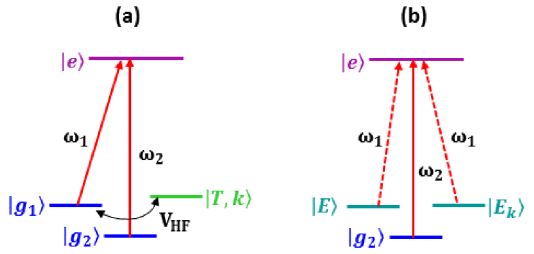

FIG. 6: Level schemes in (a) "bare-state" and (b) "continuum-dressed-state" bases. $|g_1\rangle$, $|g_2\rangle$, and $|e\rangle$ are the bare molecular states in the energetically closed (singlet) channel. $|T, k\rangle$ is a bare continuum state in the open (triplet) channel. The hyperfine interaction V_{HF} couples the bare molecular state $|g_1\rangle$ and the continuum states $|T, k\rangle$, creating the "continuum-dressed" bound state $|E\rangle$ and the (Feshbach resonance) scattering state $|E_k\rangle$.

continuum-dressed state model that fits our measured loss spectra in shape and magnitude, using the measured Rabi frequencies and trap parameters. A key result of this model is the prediction of the relative momentum dependence of the light-induced level shifts for both broad and narrow resonances, resolving a long-standing issue with predictions for broad resonances. Using the predicted relative momentum dependence of the scattering amplitude, the model can be used to examine optical control not only of the scattering length, but of the effective range, which will be experimentally studied in future work.

[1] P. O. Fedichev, Y. Kagan, G. V. Shlyapnikov, and T. M. Walraven, Phys. Rev. Lett. **77**, 2913 (1996).
[2] J. Bohn and P. Julienne, Phys. Rev. A **56**, 1486 (1997).
[3] F. Fatemi, K. Jones, and P. Lett, Phys. Rev. Lett. **85**, 4462 (2000).
[4] K. Enomoto, K. Kasa, M. Kitagawa, and Y. Takahashi, Phys. Rev. Lett. **101**, 203201 (2008).
[5] M. Theis, G. Thalhammer, K. Winkler, M. Hellwig, R. Grimm, and J. H. Denschlag, Phys. Rev. Lett. **93**, 123001 (2004).
[6] R. Yamazaki, S. Taie, S. Sugawa, and Y. Takahashi, Phys. Rev. Lett. **105**, 050405 (2010).
[7] D. M. Bauer, M. Lettner, C. Vo, G. Rempe, and S. Dürr, Nat. Phys. **5**, 339 (2009).
[8] Z. Fu, P. Wang, L. Huang, Z. Meng, H. Hu, and J. Zhang, Phys. Rev. A **88**, 041601 (2013).
[9] L. W. Clark, L.-C. Ha, C.-Y. Xu, and C. Chin, Phys. Rev. Lett. **115**, 155301 (2015).
[10] G. Thalhammer, M. Theis, K. Winkler, R. Grimm, and J. H. Denschlag, Phys. Rev. A **71**, 033403 (2005).
[11] H. Wu and J. E. Thomas, Phys. Rev. Lett. **108**, 010401 (2012).
[12] H. Wu and J. E. Thomas, Phys. Rev. A **86**, 063625 (2012).
[13] M. Semczuk, W. Gunton, W. Bowden, and K. W. Madi-

son, Phys. Rev. Lett. **113**, 055302 (2014).
[14] S. E. Harris, Physics Today **50**, 36 (1997).
[15] D. M. Bauer, Ph.D. thesis, Max-Planck-Institut für Quantenoptik, Garching and Physik Department, Technische Universitat München (2009).
[16] See the Supplemental Material for a description of the experimental methods and the continuum-dressed state model, which includes Refs. [20–23].
[17] G. Zürn, T. Lompe, A. N. Wenz, S. Jochim, P. S. Julienne, and J. M. Hutson, Phys. Rev. Lett. **110**, 135301 (2013).
[18] M. Bartenstein, A. Altmeyer, S. Riedl, R. Geursen, S. Jochim, C. Chin, J. H. Denschlag, R. Grimm, A. Simoni, E. Tiesinga, et al., Phys. Rev. Lett. **94**, 103201 (2005).
[19] E. L. Hazlett, Y. Zhang, R. W. Stites, and K. M. O'Hara, Phys. Rev. Lett. **108**, 045304 (2012).
[20] G. M. Falco and H. T. C. Stoof, Phys. Rev. A **71**, 063614 (2015).
[21] J. E. Thomas, A. Turlapov, and J. Kinast, Phys. Rev. Lett. **95**, 120402 (2005).
[22] R. Côté and A. Dalgarno, J. Mol. Spectr. **195**, 236 (1999).
[23] R. Côté, Ph.D. thesis, Massachusetts Institute of Technology (1995).

Supplemental Material

Theory

To compare the measured loss spectra with predictions, we find the two-field optically-induced change in the two-body scattering properties of an ultra-cold atomic gas near a magnetic Feshbach resonance. The scattering length and effective range are determined by the relative-momentum-dependent two-body scattering amplitude,

$$f = \frac{e^{2i\delta_s(k)} - 1}{2ik} = \frac{|a_{bg}|}{x\cot\delta_s(x) - ix}, \tag{1}$$

where $\hbar k$ is the relative momentum and the total scattering phase shift $\delta_s(k) = \Delta(k) + \Phi(k)$ is found from

$$\begin{aligned} x\cot\delta_s(x) &= \frac{x\cot\Delta(x)\,x\cot\Phi(x) - x^2}{x\cot\Phi(x) + x\cot\Delta(x)} \\ &\equiv q'(x) + iq''(x). \end{aligned} \tag{2}$$

In Eqs. 1 and 2, we have defined the dimensionless momentum $x = k|a_{bg}|$, with $a_{bg} < 0$ the background scattering length. $\Delta(x)$ arises from the background Feshbach resonance, (Eq. 3 below) while $\Phi(x)$ arises from the optical fields (Eq. 8 below). For later use, we have defined the real and imaginary parts of $x\cot\delta_s(x)$, $q'(x)$ and $q''(x)$, which determine all of the optically-controlled scattering parameters.

The phase shifts Δ and Φ are determined from the scattering state in the continuum dressed state basis, comprising the dressed bound state $|E\rangle$, the Feshbach resonance continuum state $|E_k\rangle$, and the singlet states $|g_2\rangle$ and $|e\rangle$, as shown Fig. 6b of the main text. This method enables adiabatic elimination of the excited electronic state $|e\rangle$ amplitude, even for broad Feshbach resonances where the hyperfine coupling constant is large, as noted above, provided that the Rabi frequencies are not too large. From the asymptotic ($r \to \infty$) scattering state, we determine the scattering phase shift $\delta_s(k)$ using a method analogous to Ref. [12] with $\langle r|E_k\rangle \to \sin[kr+\Delta(k)]/(kr\sqrt{V})$ playing the role of the background triplet continuum states $\langle r|k\rangle$.

In the absence of optical fields ($\Omega_1 \to 0$), the model presented in the Appendix of Ref. [12] determines the Feshbach resonance continuum states with $E_k = E_T + \hbar k^2/m \geq E_T$, yielding

$$x\cot\Delta(x) = \frac{\tilde{\Delta}_0 - \epsilon\,x^2}{1 + \tilde{\Delta}_0 - \epsilon\,x^2}. \tag{3}$$

where $\tilde{\Delta}_0 \equiv (B - B_\infty)/\Delta B$ is the detuning for the magnetic Feshbach resonance and $\epsilon \equiv E_{bg}/(2\mu_B\Delta B)$, with $E_{bg} = \hbar^2/(ma_{bg}^2)$, m the atom mass, and μ_B the Bohr magneton. With Ω_1 defined as the Rabi frequency for the singlet $|g_1\rangle \to |e\rangle$ transition in Fig. 6a of the main text, the Rabi frequency for an optical transition from $|E_k\rangle$ to $|e\rangle$ in Fig. 6b of the main text is $\Omega_1\,|\langle g_1|E_k\rangle|$, where

$$|\langle g_1|E_k\rangle|^2 = \frac{\epsilon|a_{bg}|^3}{2\pi^2}\,L(\tilde{\Delta}_0, x), \tag{4}$$

with

$$L(\tilde{\Delta}_0, x) = \frac{1}{(\Delta_0 - \epsilon\,x^2) + x^2(1 + \Delta_0 - \epsilon\,x^2)^2}. \tag{5}$$

Using the same model, we determine the dressed bound state $|E\rangle$ by solving the Schrödinger equation for states of energy $E < E_T$, i.e., for $E = E_T - E_m\,E_{bg}$, where E_m is the dimer binding energy in units of E_{bg}. In this case, the Rabi frequency for an optical transition from $|E\rangle$ to $|e\rangle$ in Fig. 6b is $\Omega_1|\langle g_1|E\rangle|$, where

$$|\langle g_1|E\rangle|^2 = \left(1 + \frac{1}{2\epsilon}\frac{1}{\sqrt{E_m}}\frac{1}{(1+\sqrt{E_m})^2}\right)^{-1}. \tag{6}$$

The dimensionless binding energy E_m satisfies,

$$\epsilon E_m + \tilde{\Delta}_0 + \frac{\sqrt{E_m}}{1+\sqrt{E_m}} = 0, \tag{7}$$

with ϵ and $\tilde{\Delta}_0$ as defined above. Here, $\tilde{\Delta}_0 < 0$ is required for the bound state $|E\rangle$ of binding energy $E_m > 0$ to exist. Eq. 6 and Eq. 7 are equivalent to the results of Ref. [20]. One can verify by numerical integration that $|\langle g_1|E\rangle|^2 + \int_0^\infty 4\pi k^2 dk\,|\langle g_1|E_k\rangle|^2 = 1$ as it should.

Including the interaction with both optical fields, we find the asymptotic scattering state in the continuum-dressed basis, which yields the optically-induced phase

shift from

$$x\cot\Phi(x) = -\frac{\tilde{\tilde{\delta}}_e(x) + \frac{\tilde{\Omega}_1^2}{4}\frac{\hbar\gamma_e}{2\mu_B\Delta B}\,S(\tilde{\Delta}_0,x) + \frac{i}{2}}{\frac{\tilde{\Omega}_1^2}{4}\frac{\hbar\gamma_e}{2\mu_B\Delta B}\,L(\tilde{\Delta}_0,x)}. \quad (8)$$

Here, the dimensionless detunings are given in units of the spontaneous decay rate γ_e,

$$\tilde{\tilde{\delta}}_e(x) \equiv \tilde{\Delta}_e(x) + \frac{\tilde{\Omega}_2^2}{4\tilde{\delta}(x)} \quad (9)$$
$$\tilde{\Delta}_e(x) \equiv \frac{2\pi\nu_1}{\gamma_e} - \frac{2\mu_B}{\hbar\gamma_e}(B - B_{ref}) + \frac{E_{bg}}{\hbar\gamma_e}x^2$$
$$\tilde{\tilde{\delta}}(x) \equiv \frac{2\pi(\nu_2-\nu_1)}{\gamma_e} + \frac{2\mu_B}{\hbar\gamma_e}(B - B_{ref}) - \frac{E_{bg}}{\hbar\gamma_e}x^2,$$

where $\nu_1 = 0$ corresponds to a single photon $T \to e$ resonance ($\tilde{\Delta}_e = 0$) at the reference magnetic field B_{ref}. Similarly, $\nu_2 = \nu_1$ corresponds to the two-photon resonance ($\tilde{\tilde{\delta}} = 0$) for the $g_1 \to e \to g_2$ transition. The dimensionless Rabi frequency is $\tilde{\Omega}_1 \equiv \Omega_1/\gamma_e$ for the $g_1 \to e$ transition and $\tilde{\Omega}_2 \equiv \Omega_2/\gamma_e$ for the $g_2 \to e$ transition.

The numerator of Eq. 8 contains an Ω_1-dependent energy shift, with

$$\frac{S(\tilde{\Delta}_0,x)}{2\mu_B\Delta B} \equiv \mathcal{P}\int dk'\,4\pi k'^2\frac{|\langle g_1|E_{k'}\rangle|^2}{E_{k'} - E_k} - \frac{|\langle g_1|E\rangle|^2}{E_{bg}\,E_m + \frac{\hbar^2k^2}{m}}\,\Theta[B_\infty - B]. \quad (10)$$

The integral term arises from the dressed continuum states, where $E'_k - E_k = \hbar^2(k'^2 - k^2)/m$, $\mathcal{P}$ denotes a principal part ($k' \neq k$), and $|\langle g_1|E_{k'}\rangle|^2$ is given by Eq. 4. The second term arises from the dressed bound state, which exists for $B < B_\infty$. The binding energy $E_T - E = E_{bg}E_m$ is determined in units of E_{bg} using Eq. 7 and $\langle g_1|E\rangle|^2$ is given by Eq. 6.

Eq. 10 is reasonably complicated. However, for the broad $1-2$ resonance in ^{6}Li, where $\epsilon = E_{bg}/(2\mu_B\Delta B) = 0.00036 << 1$, and for the narrow $1-2$ resonance, where $\epsilon = 556 >> 1$, we find that the dimensionless shift functions can be simplified,

$$S(\tilde{\Delta}_0,x) = \frac{\tilde{\Delta}_0 + (1+\tilde{\Delta}_0)x^2}{\tilde{\Delta}_0^2 + (1+\tilde{\Delta}_0)^2x^2} \quad \text{for } \epsilon << 1$$
$$S(\tilde{\Delta}_0,x) = \frac{1}{\tilde{\Delta}_0 - \epsilon\,x^2} \quad \text{for } \epsilon >> 1. \quad (11)$$

We confirm Eq. 11 by numerical evaluation of Eq. 10 in the broad and narrow resonance limits.

The shift given by Eq. 11 for the broad resonance $\epsilon << 1$ is an important new result of the continuum-dressed state approach and leads to a k-averaged two-body loss rate constant in agreement with our experiments. In particular, it avoids the incorrect prediction of a fixed resonance in the momentum-integrated loss rate at B_∞, which arises when the narrow resonance form of the shift is incorrectly applied to describe the broad resonance.

Now we determine the two-body loss rate constant, $K_2(k)$ from the inelastic scattering cross section,

$$K_2(k) = v_{rel}\,\sigma_{inel}(k) = \frac{\hbar k}{\mu}\,\sigma_{inel}(k), \quad (12)$$

where $\mu = m/2$ is the reduced mass. For a two-component Fermi gas (where atoms in different hyperfine states are distinguishable), the optical theorem for the total scattering cross section and the definition of the elastic scattering cross section give the inelastic scattering cross section in the form

$$\sigma_{inel} = \sigma_{tot} - \sigma_{el} = \frac{4\pi}{k}\,Im[f(k)] - 4\pi|f(k)|^2. \quad (13)$$

Using Eq. 2 in Eq. 1, the scattering amplitude is $f(x) = |a_{bg}|/[q'(x) - i(x - q''(x))]$, and

$$K_2(x) = \frac{8\pi\hbar|a_{bg}|}{m}\,\frac{-q''(x)}{[q'(x)]^2 + [x - q''(x)]^2}. \quad (14)$$

The atom loss rate depends on the relative-momentum-averaged loss rate constant. For simplicity, we assume a classical Boltzmann distribution of relative momentum, which is applicable for the temperatures used in the experiments that are reported in this paper. We defer treatment of degeneracy and many-body effects to future work. For a classical gas at temperature T, the relative momentum-averaged loss rate constant is then,

$$\langle K_2\rangle = \frac{4}{\sqrt{\pi}}\int_0^\infty du\,u^2e^{-u^2}\,K_2(u\,x_0), \quad (15)$$

where $x_0 \equiv k_0|a_{bg}|$ with $\hbar k_0 = \sqrt{mk_BT}$ the thermal relative momentum.

We measure the net atom loss rate for a 50-50 mixture of two hyperfine states, denoted 1 and 2. In this case, the densities $n_1(\mathbf{r}) = n_2(\mathbf{r}) = n(\mathbf{r})/2$, where $n(\mathbf{r})$ is the total density. Then, the local loss rate is

$$\dot{n}(\mathbf{r},t) = -\frac{1}{2}\langle K_2(\mathbf{r})\rangle\,[n(\mathbf{r},t)]^2. \quad (16)$$

As the Rabi frequencies that determine K_2 generally vary in space, we include an additional position dependence in $\langle K_2\rangle$. The total loss rate constant is the sum of the independent broad and narrow contributions, $K_2 = K_{2B} + K_{2N}$, since the singlet states $|g_1\rangle_B$ and $|g_1\rangle_N$ that cause the broad and narrow Feshbach resonances comprise different combinations of total electron and nuclear-spin states, which are not optically coupled [12].

Eq. 16 gives the position-dependent loss rate, which is largest where the density is largest. To determine the total number of atoms $N(t)$ at a time t after the optical fields are turned on, we need to consider possible time-dependent changes in the spatial profile of the atom cloud, which is initially gaussian in all three directions.

For moderate atom loss, when the duration of the optical pulse is long compared to the oscillation frequencies in all three directions, the gaussian initial shape of the atomic distribution will be approximately maintained as the total number decreases. Eq. 16 can be integrated over all three directions to obtain $\dot{N}$. Assuming that the diameter of the atom cloud is small compared to the diameters of the optical beams, so that the Rabi frequencies are nearly independent of $\mathbf{r}$, we have $\dot{N} = -\Gamma N^2$, where $\Gamma = \frac{\bar{n}}{2N}\langle K_2(k)\rangle$, with $\bar{n}$ the mean density. For a gaussian atomic spatial profile, where the $1/e$ widths are $\sigma_x, \sigma_y, \sigma_z$, $\bar{n}/N = 1/[(2\pi)^{3/2}\sigma_x\sigma_y\sigma_z]$, which is independent of the atom number. In this case,

$$N(t) = \frac{N(0)}{1 + N(0)\,\Gamma t}. \tag{17}$$

For simplicity, we use Eq. 17 to predict all of the spectra shown as the red curves in Figs. 2, Figs. 3 and 4 of the main text. Although the period for motion in the z-direction is comparable to the optical pulse duration, we find that this approximation yields spectra that are in reasonably good agreement with all of the data.

Experiment

The method for generating the optical fields for the two-field optical technique is shown in Fig. 7. The frequency of the reference laser L_R is stabilized by a PDH lock to the FP cavity. The FP cavity is locked to the error voltage generated from the iodine saturation absorption signal, using a beam from the reference laser L_R.

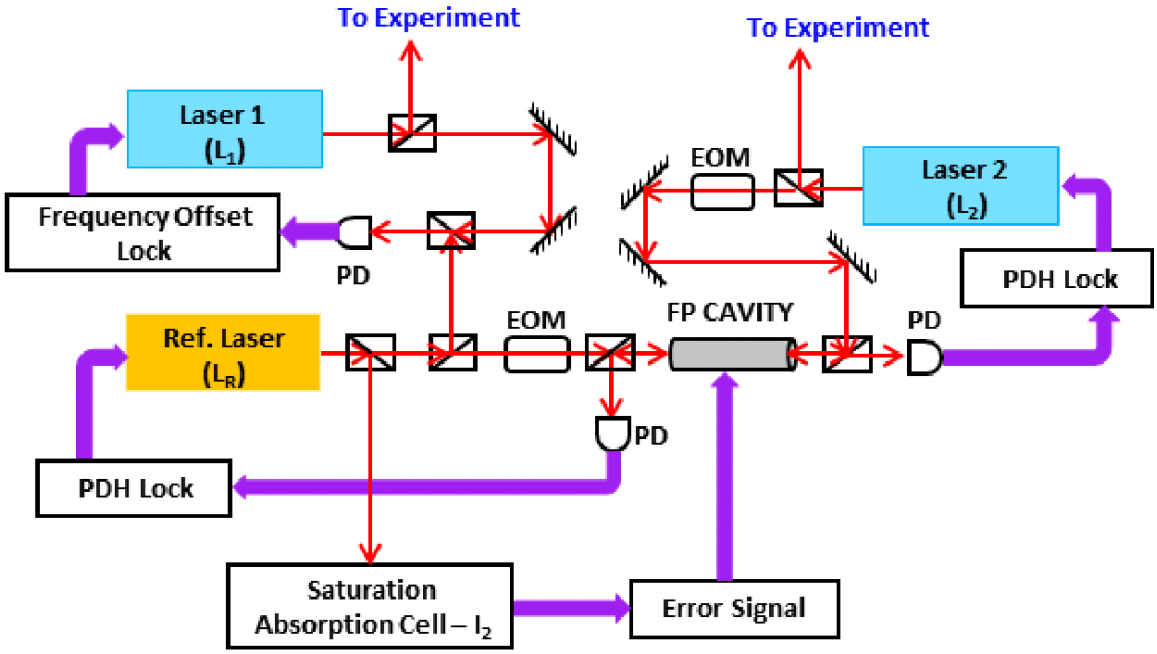

FIG. 7: Diode laser system for two-field optical control. L_R provides the frequency reference for the diode lasers L_1 and L_2 that generate the optical frequencies ω_1 and ω_2, near 673.2 nm, which excite molecular transitions from the ^{6}Li singlet molecular vibrational ground states $v = 38$ and $v = 37$, respectively.

The main advantage of this setup is that it exploits the high bandwidth lock of the PDH technique to minimize the fast jitter of the diode lasers and simultaneously provides an absolute frequency reference. Laser L_1 with frequency ω_1 is frequency offset locked to the reference laser and generates the optical field for the $v = 38$ to $v = 68$ transition. Laser L_2 with frequency ω_2 is locked to a different mode of the cavity and generates the optical field for the $v = 37$ to $v' = 68$ transition which is approximately 57 GHz higher in frequency from the $v = 38$ to $v' = 68$ transition. The relative frequency jitter between the lasers is $\Delta\nu < 50$ kHz and the absolute frequency

stability is <100 kHz. As the optical linewidth of the molecular transitions is $\gamma_e = 2\pi \times 11.8$ MHz, the absolute stability is not as critical as the relative stability, which limits the effective linewidth of the ground state coherence created by the two-field method.

Determination of the trap frequencies

For the CO_2 laser trap alone, the trap frequencies for the x, y and z directions are determined by parametric resonance. However, the intense ω_2 beam creates a red-detuned optical dipole trap and provides additional axial (z) confinement for the atom cloud, with negligible change in the transverse x, y confinement. To determine the correct mean atom density, it is important to measure the ω_z trap frequency including the effect of the ω_2 beam on the atoms. For the two-beam trap, we find that parametric resonance does not yield a high precision measurement of ω_z. Instead, we use cloud size measurements to find the total trap frequency ω_{zt}, arising from combined the CO_2 laser and ω_2 beam potentials. The ω_1 beam is turned off throughout the measurement. After forced evaporation in the CO_2 laser trap near 832 G and re-raising the trap to full depth, the ω_2 beam is adiabatically turned on over 30 ms. Then both the CO_2 laser and ω_2 beams are abruptly turned off simultaneously and the atoms are imaged after as short time of flight to determine the $1/e$ size σ_{zi} of the cloud just before release. The same procedure is repeated again, but this time, only the ω_2 beam is abruptly extinguished, so that the atoms are released from the ω_2 trap into the CO_2 laser trap, where the axial frequency is $\omega_z < \omega_{zt}$. After a hold time of 200 ms, the atom cloud reaches equilibrium and is imaged to determine its final axial width σ_{zf} in the CO_2 laser trap alone. From σ_{zi} and σ_{zf}, we determine ω_{zt} using energy conservation as follows.

Just before the ω_2 beam is extinguished, the mean z-potential energy per atom is $\frac{1}{2}m\omega_{zt}^2\langle z^2\rangle$, where $\langle z^2\rangle = \frac{\sigma_z^2}{2}$ is the mean square cloud size. As the pressure is isotropic, the total potential energy of the atoms taking into account all three directions is $\frac{3}{2}m\omega_{zt}^2\frac{\sigma_{zi}^2}{2}$. According to virial theorem [21], the mean internal energy of a unitary gas (near 832 G) is equal to the mean potential energy. Hence the internal energy of the gas at the time of release is also $\frac{3}{2}m\omega_{zt}^2\frac{\sigma_{zi}^2}{2}$. Just after extinguishing the ω_2 beam, the potential energy of the atoms (in the CO_2 laser trap alone) is $\frac{3}{2}m\omega_z^2\frac{\sigma_{zi}^2}{2}$, since σ_{zi} has not changed. The total energy of the atoms immediately after the ω_2 beam is turned off is then $E_{ti} = \frac{3}{2}m\omega_{zt}^2\frac{\sigma_{zi}^2}{2} + \frac{3}{2}m\omega_z^2\frac{\sigma_{zi}^2}{2}$. After reaching equilibrium, the total energy of the atoms in the CO_2 laser trap alone is twice the mean potential energy, $E_{tf} = 3m\omega_z^2\frac{\sigma_{zf}^2}{2}$, according to the virial theorem. By conservation of energy $E_{ti} = E_{tf}$,

$$\omega_{zt}^2 = \omega_z^2\left(2\frac{\sigma_{zf}^2}{\sigma_{zi}^2} - 1\right), \tag{18}$$

which gives ω_{zt} in terms of the CO_2 laser trap axial frequency, ω_z.

The combined trap frequency ω_{zt} determines the initial temperature T of the cloud in the total trapping potential (before release) using $k_BT = m\omega_{zt}^2\langle z^2\rangle = m\omega_{zt}^2\frac{\sigma_{zi}^2}{2}$. The cloud sizes in the x and y dimensions are then easily found from $\omega_x^2\sigma_{xi}^2 = \omega_y^2\sigma_{yi}^2 = \omega_{zt}^2\sigma_{zi}^2$, yielding $\bar{n}/N$.

Determination of the Rabi frequencies

We first estimate the Rabi frequency Ω_1 from the predicted electric dipole transition matrix element. In ^{6}Li, $|g_1\rangle$ is the $^1\Sigma_g^+$ $(N = 0)$ $v = 38$, vibrational state, which is responsible for the Feshbach resonance. Starting from that state, the best Franck-Condon factor [22] arises for an optical transition to the excited $A^1\Sigma_u^+$ $(N = 1)$ $v' = 68$ vibrational state, which we take as $|e\rangle$. For the two-field experiments, we take $|g_2\rangle$ to be the $v = 37$ vibrational state, which is essentially uncoupled to the triplet state, as it lies $\simeq 57$ GHz below the resonant state. For the $v = 38 \rightarrow v' = 68$ transition, the predicted oscillator strength is $f_{eg} = 0.034$ [22]. We find that the corresponding Rabi frequency is $\Omega_1 = 2\pi \times 5.6\,\mathrm{MHz}\sqrt{I}$, where I is the intensity of the optical beam given in mW/mm^2.

We measure the atom number, the temperature, the diameter and power of the ω_1 beam. For spatially uniform illumination, we use an ω_1 beam with a $1/e^2$ intensity radius of $750\,\mu$m, large compared to the size of the trapped cloud $(65 - 75\,\mu\mathrm{m})$. Using the measured values, we fit *all* of the loss suppression data shown in Fig. 3 [a,b,c] of the main text using $\Omega_1 = 2\pi \times c_1\,\mathrm{MHz}\sqrt{I}$, with $c_1 = 5.45(0.10)$. The measured Rabi frequency is in good agreement with the value 5.6 predicted using the Franck-Condon factors, based on the vibrational wave functions obtained from the molecular potentials [22]. For Fig. 2 [a,b,c] and Fig. 4 of the main text, we find a smaller value $c_1 = 5.1$, most likely due to imperfect overlap of the Ω_1 beam with the atom cloud.

Using $\Omega_1 = 2\pi \times 5.1\,\mathrm{MHz}\sqrt{I}$, we see from Fig. 2 [a,b,c] of the main text that the continuum-dressed state model correctly predicts all three shifts of the narrow resonance, which is the dominant factor in determining c_1. Further, for all three spectra, the amplitude and widths for both the broad and narrow resonances are correctly predicted without further adjustment. As the shift depends on Ω_1^2 while the magnitudes of the loss rates depend on the product $\Omega_1^2\,|\langle g_1|E_k\rangle|^2$, the good agreement in the shape of the spectra confirms the transition strengths and momentum-dependent shifts predicted by

the continuum-dressed state model over the range from 540 G to 840 G.

For the loss-suppression measurements, we find the additional Rabi frequency for the ω_2 beam, $\Omega_2 = 2\pi \times c_2\,\mathrm{MHz}\sqrt{I}$. Here, the $1/e^2$ radius of the ω_2 beam is 160 μm along the z-axis and 70 μm along the x-axis. Using the data of Fig. [3] of the main text, we find $c_2 = 0.14$, in reasonable agreement with the predicted value of 0.17 for the very weak $v = 37 \to v' = 68$ transition [23].